Hybrid AC/DC hub for integrating onshore wind power and interconnecting onshore and offshore DC networks

Kai Huang[1], *Wang Xiang*[1*], *Lie Xu*[1], *Yi Wang*[2]

[1] Department of Electronic and Electrical Engineering, University of Strathclyde, G1 1XW, Glasgow, UK.
[2] State Key Laboratory of Alternate Electrical Power System with Renewable Energy Sources, North China Electric Power University, Baoding 071003, People's Republic of China
[*] w.xiang@strath.ac.uk

Abstract: A hybrid AC/DC hub is proposed in this paper, where a modular multilevel converter (MMC) and a line-commutated converter (LCC) are paralleled at the AC side to integrate onshore wind power, and connected in series at the DC sides to interconnect two DC networks with different voltages. The hybrid AC/DC hub facilities wind power integration and DC network interconnection with reduced converter ratings and power losses when compared with the 'conventional' approach using DC-DC converters. To investigate the design requirement and performance of the hybrid AC/DC hub, power flow analysis is assessed to evaluate the converter power rating requirement. To ride through DC faults at either side of the interconnected DC networks, a coordinated DC fault protection for the hybrid AC/DC hub is proposed and studied. Simulation results in PSCAD/EMTDC verify the feasibility and effectiveness of the proposed control and protection of the hybrid AC/DC hub under power flow change, AC and DC fault conditions.

1. Introduction

Renewable and sustainable energy utilization has been well acknowledged as one of the most promising solutions to mitigate the climate crisis. Among various renewable energies, wind energy is considered the most developed and mature technology. By the end of 2018, 591 GW wind power has been installed world widely onshore and offshore [1].

For countries like China, India and USA, onshore wind power exploitation still plays a leading role with many large wind farms currently being developed. Transmitting power generated from large onshore wind farms to load centers over long distance, line commutated converter based HVDC (LCC-HVDC) technologies are being used, e.g. in China, several LCC-HVDC links at ±500 kV and ±800kV have been commissioned to transmit onshore wind power over 1000km [2]. In the meantime, many offshore wind farms have been installed or under construction, e.g. in Europe, modular multilevel converter based HVDC (MMC-HVDC) technologies at up to ±320 kV have been used for their grid connection [3][4].

To improve the transmission efficiency, onshore and offshore HVDC systems could be connected to existing DC networks that directly supply load centers. Due to the different voltage ratings between overhead line HVDC (e.g. onshore LCC-HVDC) and offshore MMC-HVDC systems, DC-DC converters are required to interconnect the two systems. The DC-DC converters can be galvanic isolated or non-isolated [5][6]. Several isolated topologies of DC-DC converters have been proposed, such as the modular multilevel dual-active bridge (DAB) and the inductor-capacitor-inductor (LCL) based DC-DC converters, both of which offer independent AC-DC conversion and inherent DC fault tolerate capability [7][8]. However, they require two AC/DC conversion stages, resulting in higher converter power rating and operating power loss.

The non-isolated DC-DC converter without full DC-AC-DC conversion has been proposed as an efficient alternative. The MMC based DC autotransformer (DC AUTO) is one of the most attractive and feasible solutions [9][10]. In a DC AUTO, part of DC power is transferred through the direct electrical connection between the interconnected converters, leading to reduced converter capacity and power losses. However, to achieve bidirectional fault blocking capability, the half-bridge submodules should be replaced by full-bridge or self-blocking counterparts [11], increasing costs and losses.

From the DC AUTO concept, several alternative unidirectional topologies for specified applications have been proposed to further minimize the costs and losses [12] However, they are not suitable for interconnecting DC networks requiring power reversal operation. Combined with a three-switch submodule circuit and series-connected thyristors and diodes, a hybrid non-isolated topology was proposed for DC network interconnection, which presents lower capital cost, small footprint and power losses [13]. However, performance during DC fault needs further analysis.

Therefore, a new hybrid AC/DC hub (Hybrid Hub) configuration consisted of LCC and MMC technologies is proposed in this paper for integrating onshore wind power and interconnecting onshore and offshore DC networks. In the Hybrid Hub, the onshore wind farm is directly connected to the LCC, and a MMC is connected in series between the LCC (higher DC voltage side) and DC terminals of the offshore DC network (lower DC voltage side). The Hybrid Hub can be implemented in windy areas near the coast, such as North China and South Scotland. The main contributions of this paper are as follows:

- A Hybrid Hub concept is proposed to interconnect onshore and offshore DC networks with different voltage levels, and to integrate onshore wind farms through the AC terminal. Compared with the 'conventional' interconnection approach using DC-DC converters, in the proposed Hybrid Hub, part of the power from the offshore DC network can be transmitted to the onshore DC network directly, therefore, significantly reducing the costs and power losses of converters.
- Detailed fault ride-through strategies for the Hybrid Hub are investigated. To avoid overcurrent during DC faults on submarine cable or overhead lines (OHLs), additional bidirectional thyristors associated with coordinated

current based DC fault detection algorithms are proposed to protect the converters from breakdown during DC faults on either high voltage or low voltage side.

- Comprehensive operating conditions of the interconnection system are analysed. Besides the normal operation of transmitting power from the offshore DC network to the onshore DC network, the power absorbing scenario of offshore DC network is investigated. It is found that the Hybrid Hub can provide active power to the offshore DC network, which enables the black start of offshore DC network from the onshore DC network.

This paper is organised as follows. Section 2 depicts the topology and power flow analysis of the Hybrid Hub. Section 3 presents its system layout and control principle. A comprehensive DC fault protection scheme for the Hybrid Hub is proposed in Section 4. Simulation validations on power flow change, DC fault and AC fault responses (including the study of AC fault ride-through capability) of the Hybrid Hub are provided in Section 5. Conclusions are drawn in Section 6.

2. System Topology and Power Flow Analysis

2.1. Envisaged Application Scenario

Fig. 1 illustrates an envisaged application scenario to interconnect onshore and offshore DC networks. An onshore wind farm is integrated with the local AC grid, where an LCC is used to transmit the power to the DC network with higher-voltage (HV) E_2. The DC power at the HV side is transmitted to the load center through long-distance OHLs. The DC circuit breaker (DCCB) is installed between the LCC and MMC_2 to isolate DC fault. An existing offshore DC network with a lower-voltage (LV) E_1 is connected to the onshore DC system through submarine cables. Due to the different DC voltages, a DC-DC converter (shown as the front-to-front (F2F) type [14]) is required for this interconnection to step up the voltage from E_1 to E_2. Alternative DC-DC converter configurations, e.g. a DC AUTO might be used instead of the F2F one to reduce converter power rating and power loss. However, additional submodules should be employed in the DC AUTO converters to achieve bidirectional DC fault isolating capability [9].

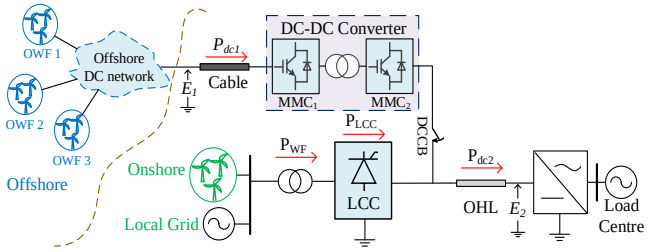

Fig. 1. *Mono-polar topology of the envisaged scenario for DC network interconnection.*

2.2. Topology of the Hybrid Hub

Fig. 2 shows the diagram of using the proposed Hybrid Hub for the envisaged application scenario. For the convenience of power flow analysis, the onshore wind farm and the local AC grid is simplified as an AC system (AC_{WF}). The AC terminals of the MMC and LCC are interconnected to the onshore AC system through AC transformers. The offshore and onshore HVDC systems marked as DC systems E_1 and E_2, respectively, are connected through the DC side of the MMC. The output of the LCC is connected to the DC terminal of E_2 through OHLs. Neglecting the voltage drops on the transmission lines, the DC voltage of the MMC is equal to the voltage difference between E_2 and E_1 under steady-state.

In comparison with the approach shown in Fig. 1, the direct electrical connection between converters is achieved in this hybrid system. The power exchange between E_1 and E_2 can be achieved through the MMC and LCC on the AC side. In addition, a DCCB is now located between the MMC and LCC terminals to improve DC fault protection, as will be detailed in Section 5.

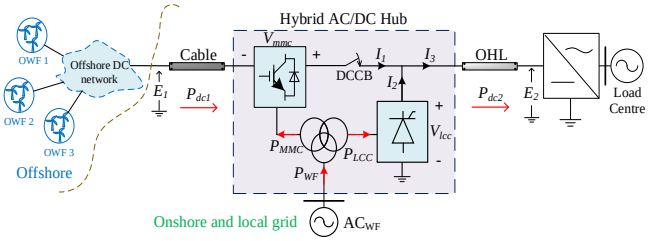

Fig. 2. *Simplified mono-polar configuration of the proposed Hybrid Hub.*

2.3. Power Flow Analysis of the Hybrid Hub

Taking power transferring from E_1 (LV) to E_2 (HV) as the positive direction, as shown in Fig. 2, the DC voltage stepping ratio and power transfer ratio between E_1 and AC_{WF} are defined as

$$\begin{cases} m = E_2 / E_1, & m > 1 \\ k = P_{dc1} / P_{WF}, & k > 0 \end{cases}. \tag{1}$$

where P_{dc1} is the rated active power from cable-based HVDC system and P_{WF} is the rated active power from AC_{WF}.

Neglecting the power losses of the transmission lines and converters, the total power transferred to the HV side of the HVDC system is

$$P_{dc2} = P_{dc1} + P_{WF} = (k+1)P_{WF}. \tag{2}$$

The DC currents at the LV side and HV side are given respectively as

$$I_1 = P_{dc1} / E_1,\ I_3 = P_{dc2} / E_2. \tag{3}$$

The DC current of the LCC is

$$I_2 = I_3 - I_1 = (P_{dc2} / E_2 - P_{dc1} / E_1). \tag{4}$$

Neglecting the voltage drop on the DC transmission lines, the DC voltages of the LCC and MMC are

$$\begin{cases} V_{LCC} = E_2 \\ V_{MMC} = E_2 - E_1 \end{cases}. \tag{5}$$

Therefore, the active power transferred by the MMC is

$$\begin{aligned} P_{MMC} &= V_{MMC} I_1 = (E_2 - E_1)\frac{P_{dc1}}{E_1} \\ &= kP_{WF}(m-1). \end{aligned} \tag{6}$$

Similarly, the active power of LCC is

$$\begin{aligned} P_{LCC} &= V_{LCC} I_2 = V_{LCC}(I_3 - I_1) \\ &= E_2(P_{dc2} / E_2 - P_{dc1} / E_1) = (k+1-km)P_{WF}. \end{aligned} \tag{7}$$

The power transferred by the direct electrical connection (without being converted by either the MMC or the LCC) is

$$P_{direct} = E_2 I_1 = mkP_{WF}. \tag{8}$$

The total power rating of the LCC and MMC can be

obtained by adding (6) and (7) as

$$P_{h\_hub} = P_{LCC} + P_{MMC} = P_{WF}. \quad (9)$$

The total power transferred by the MMC and LCC can also be obtained from a point of view of active power balance. The active power of AC_{WF} which is equal to P_{WF}, flowing into the MMC and LCC separately, as shown in Fig. 2.

The total power rating of the 'conventional' F2F DC network interconnection as shown in Fig. 1 is

$$\begin{aligned} P_{con} &= P_{MMC} + P_{LCC} = 2P_{dc1} + P_{WF} \\ &= (2k+1)P_{WF} > P_{h\_hub}. \end{aligned} \quad (10)$$

If a F2F DC-DC converter in Fig. 1 is replaced by the DC AUTO based on [9], the total power rating is

$$\begin{aligned} P_{AT} &= 2kP_{WF}(1-1/m) + P_{WF} \\ &= (2k+1-2k/m)P_{WF} > P_{h\_hub}. \end{aligned} \quad (11)$$

It is shown from (9) and (10) that the total used converter power rating of the Hybrid Hub is always lower than those using DC-DC converters. Fig. 3 compares the total power ratings of three operation scenarios and the efficiency advantage of the Hybrid Hub is clearly demonstrated, especially for higher k and m. For example, with m=2 (DC voltage ratio) and k=5 (active power ratio between the onshore wind power and the power from offshore DC network), the total converter ratings of the F2F and AUTO schemes are 11 and 6 times of that of the proposed Hybrid Hub.

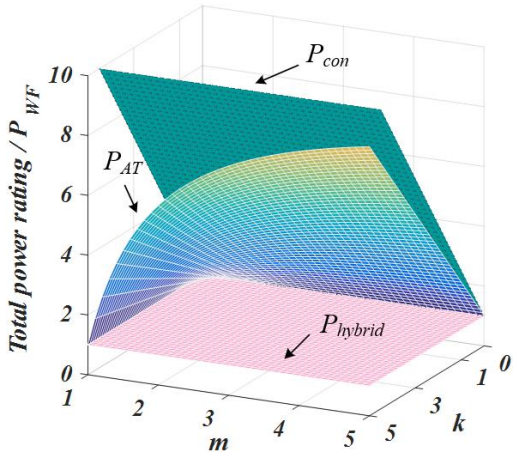

Fig. 3. *Relationship of total power ratings for different operation scenarios with different power ratio k and DC voltage ratio m.*

In addition, converter cost and power loss of LCC for high power schemes are lower than that of MMC [15]. According to (6) and (7), when k is fixed, lower m leads to smaller converter rating of MMC and larger that of LCC, which contributes to higher overall efficiency and lower cost of the Hybrid Hub.

2.4. Analysis of Power Reversal to the Offshore HVDC System.

Power reversal to the offshore HVDC system may be required for the startup of the offshore DC network, and providing power supply to other loads in the offshore systems during wind farm shutdown.

As the active power of the LCC always keeps the same direction due to its unidirectional characteristic, it continuously receives power from the AC network connecting to the MMC and onshore AC system. The reversed power to the LV side is determined by the power from the HV side and AC side. Considering the MMC's power ratings, the reversed power to the LV side can be up to $P_{MMC}E_1/(E_2-E_1)$. Depending on the power flow direction of the HV side, Fig. 4 shows power transmitted to the offshore LV side of the Hybrid Hub in two scenarios. The red arrows show that both the LCC and HV networks feed power to the LV side whereas the green dotted arrows show the case when the LCC supplies power to both the LV and HV sides.

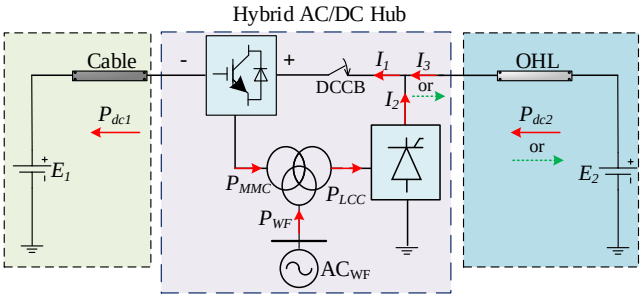

Fig. 4. *Current and power directions in two power reversal situations: E_2 transmits power and E_2 receives power (green dotted arrows).*

3. Control Principle

3.1. Control of the MMC

The layout and control principle of the Hybrid Hub are shown in Fig. 5 using single-phase representation. As shown, each arm of the MMC constitutes an arm inductor and N submodules (SMs) which can be half-bridge sub-modules (HBSMs), full-bridge sub-modules (FBSMs) or combination of them (hybrid scheme).

The synchronous d-q reference frame is used in the MMC AC current controllers [16]. For the different control arrangements of the offshore DC network, the outer d-axis controller has two control modes as required to adjust the positive sequence d-axis current order. If the DC voltage of the LV side is controlled by the offshore DC network, the MMC power control is used to regulate the transmitted DC power from the LV side. Alternatively, if the transmitted DC power from the LV side is regulated by the offshore system, the MMC voltage control is activated to control the DC voltage of the LV side. Similarly, the outer reactive power controller produces positive sequence q-axis current order based on the reactive power requirement (can provide reactive power compensation for the LCC). The negative sequence current order can be simply set at zero or other value based on the condition of the connected AC network. Since it is not the focus of this paper, no further description is provided here.

Both positive and negative sequence currents are regulated in the inner current controllers, which generate AC components of the modulation functions and limit current contribution to AC faults [17]. The voltage distribution of MMC across the three-phase legs and the upper and lower arms of each phase leg will be regulated equally by horizontal and vertical capacitor voltage balancing controllers, respectively [17]. The 2nd order harmonic currents in the arms of MMC are suppressed by the circulation current suppression controller to reduce the converter losses and the

SMs' capacitor voltage ripples.

Nearest level modulation (NLM) is used for providing gate signals to each SMs, which can closely fit the output voltage reference and reduce the switching frequency of the high DC link voltage [18].

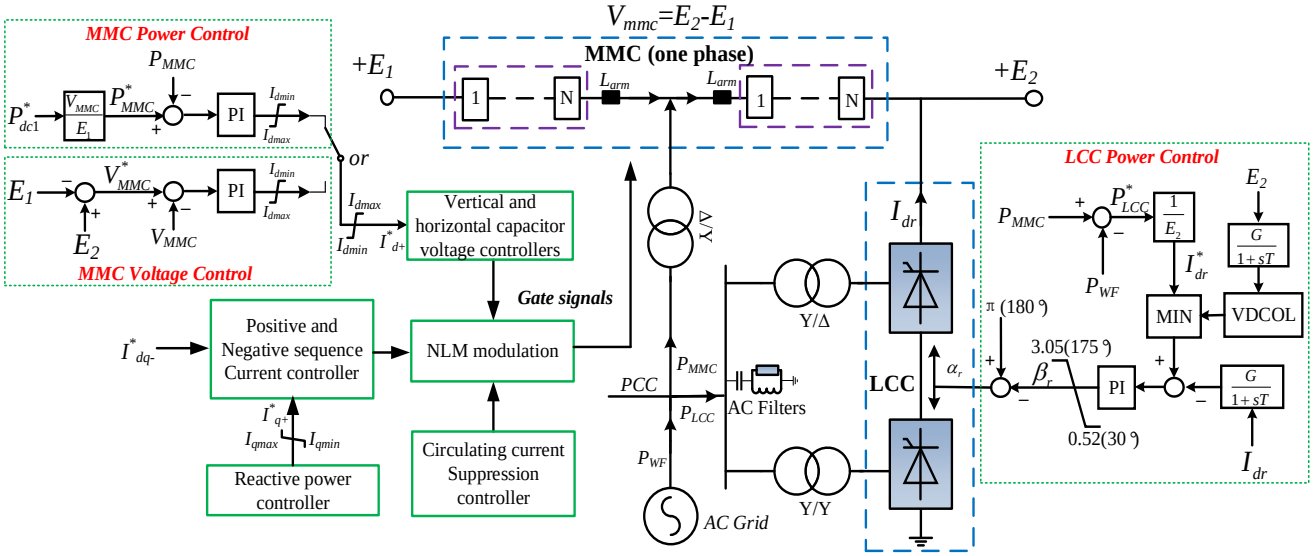

Fig. 5. *System layout and control of the Hybrid Hub.*

3.2. Control of the LCC

The rectifier LCC is composed of two six-pulse thyristor bridges in series with two corresponding transformers to form a 12-pulse converter configuration. AC filters are used to absorb AC side harmonics and to supply reactive power to the converter.

The LCC rectifier station controls the DC current to regulate the active power whereas the LCC inverter controls the DC voltage. Using the power direction definition shown in Fig. 2, the active power order of the LCC is the power difference between the required power transmission from the onshore AC system and active power absorbed by the AC side of the MMC. As shown in Fig. 5, the desired LCC power is then regulated by its DC current I_{dr}^{*} using Constant Current Control (CCC) with Voltage-Dependent Current Order Limiter (VDCOL). In normal operation, the CCC is working by comparing the measured DC current I_{dr} and I_{dr}^{*} to produce the error signal. A PI controller receives the current signal to produce the desired firing angle order α to the LCC. The VDCOL is added as an auxiliary control during fault conditions. When the DC voltage of LCC drops to a certain threshold, the DC current will be controlled to be reduced. The reduced DC current helps to improve DC voltage recovery and AC system stability as the absorbed reactive power is reduced [19].

4. DC Fault Protection

4.1. System Behaviour during DC Fault

In the event of a DC fault on either side of the Hybrid Hub, similar to the DC AUTO, the fault current will feed from the healthy DC side into the faulty DC side through the MMC due to its direct electrical connection [9].

If the MMC in the Hybrid Hub is designed to block DC faults using HBSMs and FBSMs, it has to provide the full HV side DC voltage in the event of a LV side fault to interrupt the fault current from the HV side, as shown in Fig. 6 (a). Similarly, Fig. 6 (b) shows that the MMC has to support the full LV side DC voltage to interrupt the fault current from the LV side, in the event of a DC fault on the HV side. The LCC has no influence during DC fault on either side, as it can eliminate its DC current by simply increasing the firing angle. Therefore, additional FBSMs should be inserted into the MMC depending on the voltage ratio *m*.

If DCCBs are used to isolate DC faults, the MMC has to be bypassed and the fault current will flow through the freewheeling diodes. Thus, a comprehensive DC fault protection is required to protect the whole system.

Taking into account the voltage stepping ratio level given in [6], the low stepping ratio is defined to be less than or around 1.5. Two DC fault protection schemes under high and low stepping ratios are analysed as follows.

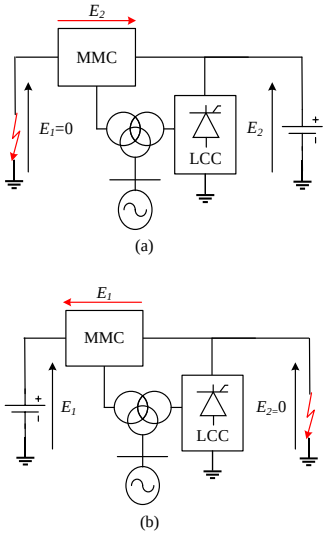

Fig. 6*. Equivalent circuits with MMC blocking during different DC faults*
(a) LV DC side fault, (b) HV DC side fault.

4.2. DC Fault Protection under High Stepping Ratio

If the voltage stepping ratio is relatively high ($m \geq 2$), i.e.

the voltage rating of MMC is also high, a hybrid MMC that composes of HBSMs and FBSMs, could be used to interrupt DC faults on either LV or HV side. Neglecting the voltage drops across the DC lines, the required capacitor voltages of the MMC and FBSMs in each arm ($V^*_{arm\_MMC}$ and $V^*_{arm\_FBSM}$) to isolate DC fault, and the DC voltage rating of the MMC in each arm (V_{arm_MMC}) without DC fault consideration are expressed as,

$$\begin{cases} V^*_{arm\_MMC} = \dfrac{E_2}{2} = \dfrac{mE_1}{2} \\ V^*_{arm\_FBSM} = \dfrac{E_1}{2} \\ V_{arm\_MMC} = (m-1)E_1 \end{cases} . \quad (12)$$

In terms of HV side faults, if $V^*_{arm\_MMC} > V_{arm\_MMC}$ (i.e. $m<2$), additional HBSMs should be inserted into each arm of the MMC to increase its voltage rating to $E_1/2$ in order to protect the MMC from submodule overvoltage.

Similarly, additional FBSMs should be inserted into each arm of the MMC if $V^*_{arm\_FBSM} > V_{arm\_MMC}$ (i.e. $m<1.5$) in the case of LV side faults. Based on these, the hybrid MMC is not a good option for DC fault protection if m is small as the required additional FBSM could lead to extremely high cost.

4.3. DC Fault Protection under Low Stepping Ratio

The Hybrid Hub with a small voltage stepping ratio (m is less than or around 1.5) will be mainly analysed in this paper since a small m has been proven to be more efficient and economical. For DC fault protection, DCCBs will be used and the MMC is bypassed during DC faults. Thus, the standard MMC with only HBSMs will be employed in the system.

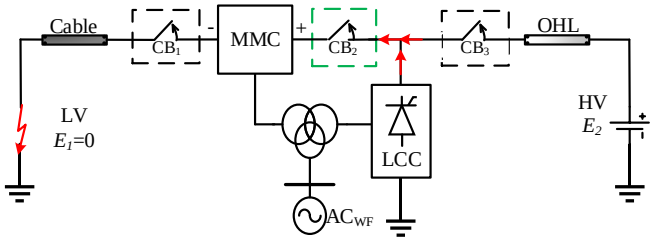

(a)

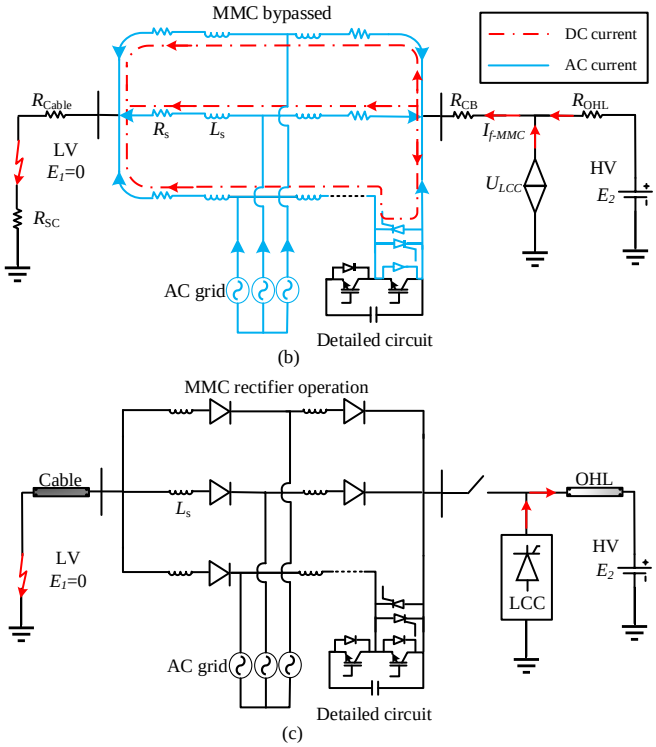

Fig. 7. *Equivalent circuits in the system and MMC during E_1 fault*
(a) different configurations of the DCCB, (b) fault current when MMC is bypassed, (c) equivalent circuit after the opening of the DCCB and bypass thyristors switched off.

In order to quickly interrupt the DC fault under the low stepping ratio, the hybrid DCCB is considered here [20]. Fig.7 (a) shows three possible locations for installing the DCCB (CB_1, CB_2 and CB_3). CB_3 is not recommended as the LCC can still transfer power to E_2 during E_1 fault if the DCCB is tured off at CB_1 or CB_2. CB_1 and CB_2 have the same effect on the DC fault isolation due to the series connection. CB_1 which is directly connected to the cable is lack of boundary effect for the boundary protection design [21]. CB_2 is more preferred as it is located at the HV side and is between MMC and LCC, where the arm inductors of the MMC and smoothing reactors can help CB_2 to limit the fault current rising rate and provide boundary effect.

In the event of LV side DC faults, the bidirectional thyristors paralleled with each SM are turned on to bypass the MMC and commutate the fault currents to flow through them, as shown in Fig. 7 (b). As shown, the transient fault current following through the MMC (thyristors) is superimposed by DC and AC sides. The fault current contributed by the DC side is large due to the DC voltage difference between the healthy side and the faulty side, which has to be interrupted by the DCCB. The fault current contributed by the AC side of the MMC is analysed in [22], which only flows through the MMC arms without any influence on the DC side.

After the opening of the hybrid DCCB, the DC fault current is interrupted. Then, the firing pulses to the thyristors will be turned off and thyristors will be turned off by the AC grid connected to the MMC [22]. The MMC operates as an uncontrolled rectifier, where the DC voltage of the MMC will be rebuilt for power recovery. The LCC keeps transmitting power to E_2, as illustrated in Fig. 7 (c). Once the DC fault is cleared, the DCCB can be re-closed and all IGBTs are

deblocked to restart the MMC.

In the event of HV side DC faults, once the fault is detected, all the thyristors in the MMC and the hybrid DCCB are turned on. The fault clearance procedure of the MMC is the same as the one on the LV side, which will not be repeated. However, different from the LV side DC fault, the firing angle of LCC is increased similar to DC fault handling by the rectifier station in a conventional LCC HVDC system [23].

4.4. Principle of Coordinated Current Protection

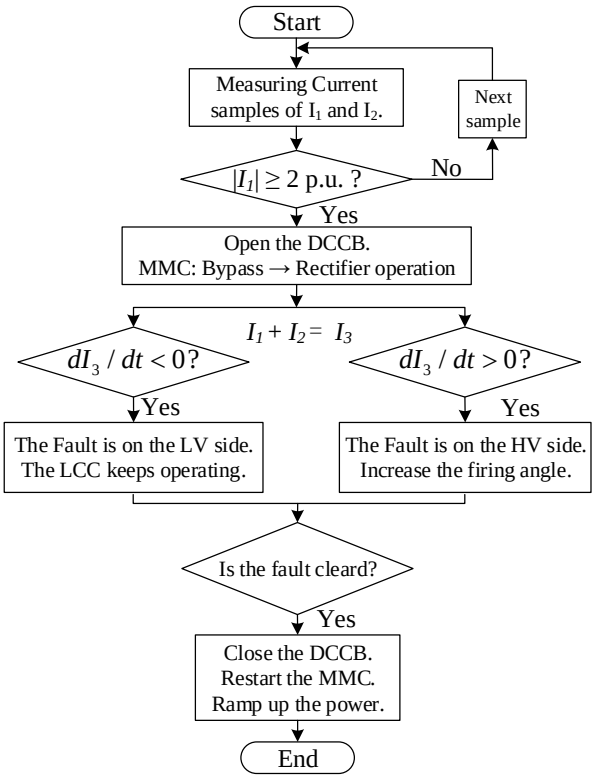

Fig. 8*. Flow chart of coordinated current protection.*

As the LCC continues operating during LV side (E_1) fault, and only one DCCB is implemented, an effective DC fault protection is necessary for the Hybrid Hub to identify the fault location on either side.

A method of coordinated current protection is proposed to accurately detect the fault side and to determine the system operation state precisely. The protection procedure is shown in Fig. 8. As indicated in Fig. 2, I_1 is the DC current of the MMC and the DCCB, the DC current of the LCC is I_2, and I_3 is the sum of I_1 and I_2.

During a DC fault, an opening command is sent to the DCCB once the absolute value of I_1 exceeds twice the rated value. At the same time, the MMC is blocked and the paralleled thyristors are turned on. When the DCCB fully opens and I_1 is extinguished, the parallel thyristors are then turned off and MMC behaves as an uncontrolled rectifier. A coordinated current protection is used to identify the fault side by comparing the current derivative value. If dI_3/dt is less than zero, the fault is on the LV side, the LCC can remain in normal operation to transfer the power from the AC side. If dI_3/dt is greater than zero, the fault is on the HV side, and the LCC should increase the firing angle to extinguish the DC fault current. After the fault is cleared, the DCCB can be reclosed to restart the MMC, the system is recovered by ramping up the power of the LCC and MMC.

5. Simulation Validations

Table 1 Parameters of MMCs

Parameters	MMC	LCC
Rated active power	300 MW	1000 MW
Rated DC voltage	180 kV	500 kV
Rated capacitor voltage of each SM	1.83 kV	—
Capacitance of each SM	11.5 mF	—
Arm inductance L_0	0.0123 H	—
Number of sub-modules per arm	100	—
DC smoothing inductance	0.05 H	0.15 H
Common bus AC voltage	250 kV	250 kV
Interfacing transformer voltage ratio	250 kV/90 kV	250 kV/250 kV

A simulation model of the circuit shown in Fig. 2 is developed in PSCAD/EMTDC to verify the efficacy of the proposed system. The Hybrid Hub is rated at +320 kV/+500 kV (i.e., m=1.56), the power transferred from AC_{WF} and E_1 are rated at 1250 MW and 500 MW (i.e., k=0.4), respectively.

The 500 kV LCC rectifier is modified from the CIGRE benchmark model [24], The equivalent averaged model is used to model the HB-MMC for faster simulation. The MMC power control is used as the DC voltage of the LV side is given in this simulation test.

The parameters of the MMC and LCC are listed in Table 1. The 100 km cable and 300 km OHL are modelled using the frequency-dependent model provided by PSCAD/EMTDC. Based on [20], the hybrid DCCB is modelled to quickly interrupt the DC fault.

5.1. Normal Operation and Power Reversal

Based on Table 1 and Section 2.3, the power transfer during normal operation can be up to 500 MW from E_1 (P_{dc1}), 1250 MW from AC_{WF} (P_{WF}) and hence 1750 MW will be received by E_2 (P_{dc2}). If the reversal power to E_1 is fully rated at 500 MW, the transferred power from AC_{WF} is 687.5 MW and hence 187.5 MW will be transmitted to E_1.

Fig. 9 shows the system responses to normal operation and power reversal. As shown in Fig. 9 (a), the DC power P_{dc1} and P_{wf} achieve steady state at 1.5 s, and are stepped to the rated reversal values at 3.0 s and ramped up again to the rated normal operation values at 4.5 s.

Fig. 9 (b) shows the active power of converters and wind farms, which follow their power order well. The total active power of through the LCC and MMC converters is 1250 MW. For comparison, the total active powers are 2250 MW and 1610 MW by using the F2F DC-DC converter and DC AUTO, respectively.

Figs. 9 (c) and (d) show the MMC arm currents and SM capacitor voltages, respectively. It can be seen that they are well controlled and balanced within their rated values during normal operation and power step changes.

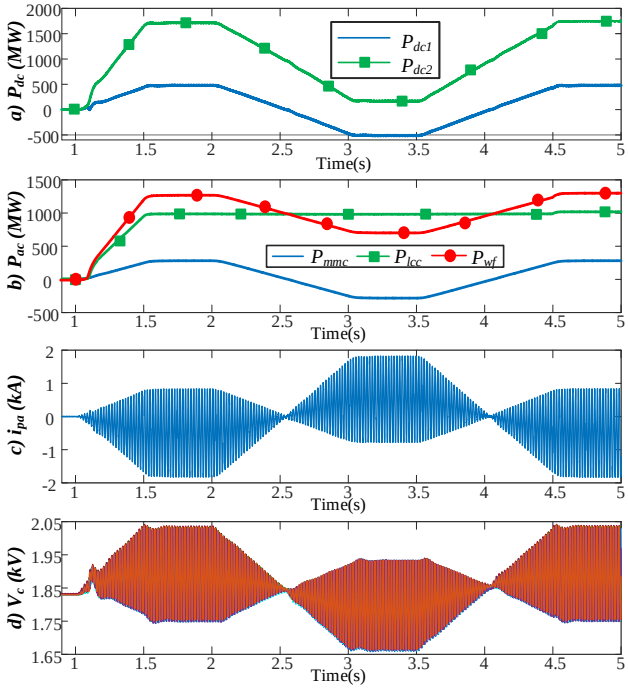

***Fig. 9**. Response to power flow change*
(a) DC power of E_1 and E_2, (b) Active power of converters and wind farm, (c) MMC arm current, (d) MMC SM capacitor voltages.

5.2. AC Fault Ride-Through

The Hybrid Hub needs to consider the capability of AC fault ride-through as these two converters are interconnected to the AC side.

On the LCC rectifier side, different from the LCC inverter, there is no commutation failure on the rectifier side during AC fault, so no converter blocking is required with no overvoltage and/or overcurrent. The transmitted active power through the LCC goes to zero during the AC fault but is restored quickly after the recovery of AC system voltage. On the MMC side, due to the closed-loop current control within the MMC control system, the fault current is limited, which has been researched in many topics [25][26].

To verify the AC fault ride-through capability of Hybrid Hub, system responses to an AC fault are shown in Fig. 10. Fig. 10 (a) shows the common bus AC voltage. A temporary three-phase to ground fault is applied at 4.0 s for 200 ms. Fig. 10 (b) shows the DC voltages of the MMC and LCC, which are remained around the rated values during AC fault. Fig. 10 (c) shows the DC currents of the converters. The DC current of the MMC (I_1) oscillates but is limited by the closed-loop current control during AC fault. The DC current of the LCC (I_2) is reduced to zero quickly during AC fault. After the fault is cleared, I_1 and I_2 are restored to the pre-fault values at 5.0 s. The arm currents of MMC are also limited by the current control at the occurrence of the AC fault, as shown in Fig. 10 (d).

In conclusion, without any specific protection schemes, the Hybrid Hub can operate securely during AC faults.

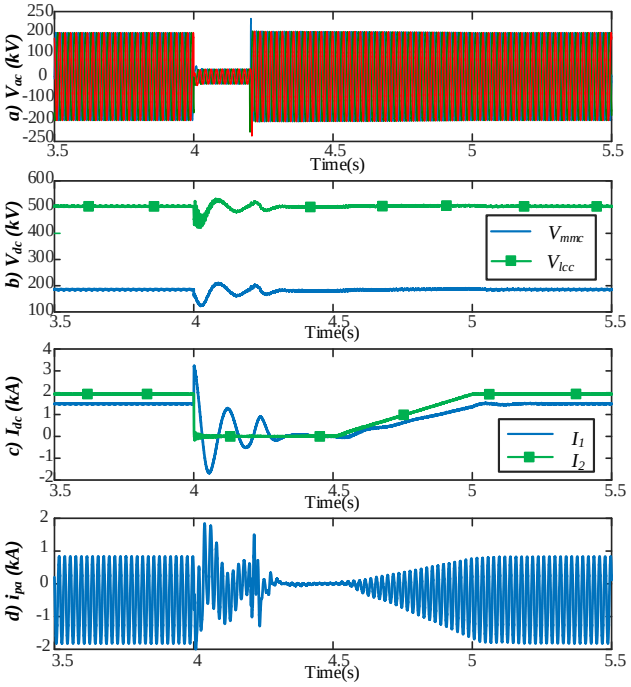

***Fig. 10**. Response to AC fault*
(a) AC voltage, (b) DC voltages of MMC and LCC, (c) DC currents, (d) MMC arm currents.

5.3. Response to DC Fault

System responses during a DC fault are shown in Figs. 11 and 12. Temporary DC faults are applied on the LV side at 2.0 s, and the HV side at 3.5 s, respectively. The proposed DC fault protection identifies the fault locations and determines the operating status of the LCC. The MMC is bypassed to protect itself during the DC faults, while the hybrid DCCB isolates the DC faults to protect the Hybrid Hub. When the DC fault is cleared, the DCCB is reclosed and the MMC and LCC are recovered to the pre-fault operation.

Fig. 11 (a) shows the DC voltages of E_1 and E_2, while Fig. 11 (b) shows the DC currents. Due to the fast tripping of the hybrid DCCB, the DC current of the MMC (I_1) drops to zero within 10 ms. As the LCC continues operating during E_1 fault, the DC current of the LCC (I_2) remains the same, whereas it is fully eliminated during E_2 fault. Fig. 11 (c) shows the current I_3, and it can be seen that, the derivative of I_3 with time is negative during E_1 fault while it is positive during E_2 fault, which proves the efficacy of the coordinated current protection.

Fig. 11 (d) shows the active power of the converters and wind farms. During E_1 fault, the active power of AC_{WF} is reduced to transfer through the LCC only while the active power of the MMC is reduced to zero. When it comes to E_2 fault, the active power of the MMC, LCC and AC_{WF} are all reduced to zero.

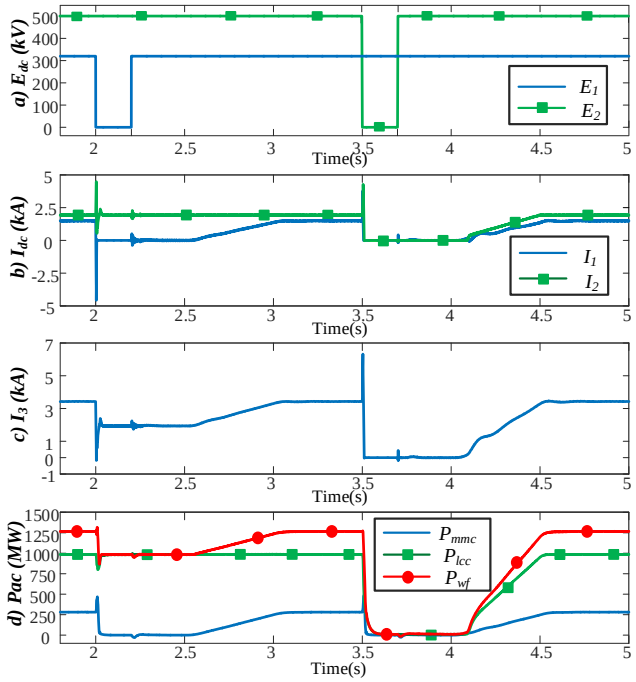

***Fig. 11**. Response to DC faults*
(a) DC voltages of E_1 and E_2, (b) Converter DC currents, (c) DC current of I_3, (d) active power of converters and wind farm.

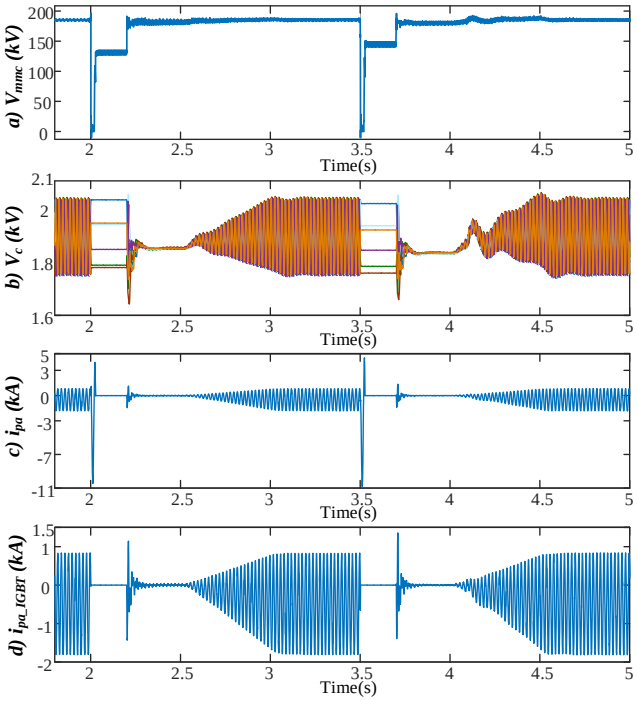

***Fig. 12**. MMC Response to DC faults*
(a) MMC DC voltage, (b) MMC capacitor voltages, (c) MMC arm currents, (d) currents through IGBTs.

Fig. 12 (a) shows the DC voltage of the MMC, in which similar results are observed during E_1 and E_2 faults. V_{mmc} drops to zero when a DC fault occurs, and then it rises below the rated value since the MMC behaves as an uncontrolled rectifier. When the fault is cleared, the MMC is enabled and V_{mmc} restores and stabilises at the rated value.

Fig. 12 (b) shows the capacitor voltages of the MMC during a DC fault. There is no capacitor overcharging observed as the capacitor voltages remain within the rated value whenever IGBTs are blocked or deblocked.

Figs. 12 (c) and (d) show the arm currents of the MMC and the currents flowing through the IGBTs, respectively. The arm overcurrents are interrupted rapidly by the DCCB, as shown in Fig. 12 (c). The MMC is bypassed quickly on detecting a DC fault on either side. Therefore, there are no overcurrents observed at the IGBTs as they are bypassed by the parallel thyristors, as shown in Fig. 12 (d).

6. Conclusions

A hybrid AC/DC hub for the integration of onshore wind power and interconnection of onshore and offshore DC networks is proposed in this paper. The topology, operation, control and fault-ride through of the Hybrid Hub is studied. Taking the integration of +320 kV HVDC, +500 kV HVDC and 250 kV AC systems as an example, the proposed Hybrid Hub significantly reduces the total required converter power rating from 2250 MW for a 'conventional' DC network interconnection to 1250 MW. It can also achieve up to 500 MW power reversal to support the offshore system. By utilising the existing AC grid of onshore system and coordinated control of the LCC and MMC, the Hybrid Hub operates stably. By considering the sign of the derivative of the DC current I_3 with time, the proposed DC fault protection scheme for the Hybrid Hub rapidly identifies and isolates the DC fault on either LV or HV side. Due to the unidirectional conduction character of the LCC rectifier and the closed-loop current control of MMC, the Hybrid Hub can also ride through AC faults. PSCAD/EMTDC simulations validate the technical feasibility of the proposed hybrid AC/DC hub for HVDC applications.

7. References

[1] GWEC Global Wind Report 2018". Accessed on: April, 2019. [Online]. Available at http://www.gwec.net/.
[2] D. Pudney, H. Voltage, and T. Sa, "A review of HVDC in China," Energize, 2012.
[3] G. Chen, M. Hao, Z. Xu, A. Vaughan, J. Cao, and H. Wang, "Review of high voltage direct current cables," CSEE J. Power Energy Syst., vol. 1, no. 2, pp. 9–21, 2015.
[4] Bin Li, Jiawei He, Ye Li, Botong Li. A review of the protection for the multi-terminal VSC-HVDC grid. Protection and Control of Modern Power Systems, 2019, 4(4): 239-249.
[5] S. J. Finney, G. P. Adam, B. W. Williams, D. Holliday, and I. A. Gowaid, "Review of dc–dc converters for multi-terminal HVDC transmission networks," IET Power Electron., vol. 9, no. 2, pp. 281–296, Feb. 2016.
[6] J. D. Paez, D. Frey, J. Maneiro, S. Bacha, and P. Dworakowski, "Overview of DC–DC Converters Dedicated to HVdc Grids," IEEE Trans. Power Deliv., vol. 34, no. 1, pp. 119–128, Feb. 2019.
[7] A. M. Omran, K. H. Ahmed, M. S. Hamad, and I. F. Al-Arabawy, "Interconnection between different DC technologies at multi-terminal HVDC network," 3rd Int. Conf. Renew. Energy Res. Appl. ICRERA 2014, pp. 295–300, 2014.
[8] M. G. Jahromi, G. Mirzaeva, and S. D. Mitchell, "Design and Control of a High-Power Low-Loss DC-DC Converter for Mining Applications," IEEE Trans. Ind. Appl., vol. 53, no. 5, pp. 5105–5114, 2017.
[9] W. Lin, "DC-DC autotransformer with bidirectional DC fault isolating capability," IEEE Trans. Power Electron., vol. 31, no. 8, pp. 5400–5410, 2016.
[10] Z. Yang et al., "Interconnection of VSC-HVDC and LCC-HVDC using DC–DC autotransformer," J. Eng., vol. 2019, no. 18, pp. 5033–5037, Jul. 2019.
[11] W. Xiang, W. Lin, T. An, J. Wen, and Y. Wu, "Equivalent Electromagnetic Transient Simulation Model and Fast Recovery Control of Overhead VSC-HVDC Based on SB-MMC," IEEE Trans.

Power Deliv., vol. 32, no. 2, pp. 778–788, Apr. 2017.
[12] M. Zhou, W. Xiang, W. Zuo, W. Lin, and J. Wen, “A Unidirectional DC-DC Autotransformer for DC Grid Application,” Energies, vol. 11, no. 3, p. 530, Mar. 2018.
[13] B. Li, X. Zhao, D. Cheng, S. Zhang, and D. Xu, “Novel Hybrid DC/DC Converter Topology for HVDC Interconnections,” IEEE Trans. Power Electron., vol. 34, no. 6, pp. 5131–5146, Jun. 2019.
[14] N. Ahmed, A. Haider, D. Van Hertem, L. Zhang, and H.-P. Nee, “Prospects and challenges of future HVDC superGrids with modular multilevel converters,” Proc. Power Electron. Appl., pp. 1–10, 2011.
[15] P. S. Jones and C. C. Davidson, “Calculation of power losses for MMC-based VSC HVDC stations,” in 2013 15th European Conference on Power Electronics and Applications (EPE), 2013, no. Mmc, pp. 1–10.
[16] L. Xu, L. Yao, and C. Sasse, “Grid Integration of Large DFIG-Based Wind Farms Using VSC Transmission,” IEEE Trans. Power Syst., vol. 22, no. 3, pp. 976–984, Aug. 2007.
[17] R. Zeng, L. Xu, L. Yao, and S. J. Finney, “Analysis and Control of Modular Multilevel Converters under Asymmetric Arm Impedance Conditions,” IEEE Trans. Ind. Electron., vol. 63, no. 1, pp. 71–81, Jan. 2016.
[18] M. Perez, J. Rodriguez, J. Pontt, and S. Kouro, “Power Distribution in Hybrid Multi-cell Converter with Nearest Level Modulation,” in 2007 IEEE International Symposium on Industrial Electronics, 2007, pp. 736–741.
[19] X. Yu, J. Yi, N. Wang, Y. Teng, and Q. Huang, “Analysis on Dynamic Response of LCC-VSC Hybrid HVDC System with AC/DC Faults,” in 2018 IEEE Innovative Smart Grid Technologies - Asia (ISGT Asia), 2018, pp. 323–327.
[20] J. Häfner and B. Jacobson, “Proactive Hybrid HVDC Breakers - A key innovation for reliable HVDC grids,” Electr. power Syst. Futur. - Integr. supergrids microgrids Int. Symp. Bol. , Italy, p. 9, 2011.
[21] W. Xiang, S. Yang, L. Xu, J. Zhang, W. Lin, and J. Wen, “A Transient Voltage-Based DC Fault Line Protection Scheme for MMC-Based DC Grid Embedding DC Breakers,” IEEE Trans. Power Deliv., vol. 34, no. 1, pp. 334–345, Feb. 2019.
[22] X. Li, Q. Song, W. Liu, H. Rao, S. Xu, and L. Li, “Protection of nonpermanent faults on DC overhead lines in MMC-based HVDC systems,” IEEE Trans. Power Deliv., vol. 28, no. 1, pp. 483–490, 2013.
[23] W. Xiang, R. Yang, C. Lin, J. Zhou, J. Wen, and W. Lin, “A Cascaded Converter Interfacing Long Distance HVDC and Back-to-Back HVDC Systems,” IEEE J. Emerg. Sel. Top. Power Electron., vol. PP, no. c, pp. 1–1, 2019.
[24] M. Szechtman, T. Wess, and C. V. Thio, “Benchmark model for HVDC system studies,” IEE Conf. Publ., no. 345, pp. 374–378, 1991.
[25] Y. Zhou, D. Jiang, J. Guo, P. Hu, and Y. Liang, “Analysis and Control of Modular Multilevel Converters Under Unbalanced Conditions,” IEEE Trans. Power Deliv., vol. 28, no. 4, pp. 1986–1995, Oct. 2013.
[26] J. W. Moon, J. W. Park, D. W. Kang, and J. M. Kim, “A Control Method of HVDC-Modular Multilevel Converter Based on Arm Current under the Unbalanced Voltage Condition,” IEEE Trans. Power Deliv., vol. 30, no. 2, pp. 529–536, 2015.